Stabilizing the spin vortex crystal phase in two-dimensional iron-based superconductors

Joseph O'Halloran, D. F. Agterberg, M. X. Chen, and M. Weinert

Phys. Rev. B **95**, 075104 — Published 2 February 2017

DOI: 10.1103/PhysRevB.95.075104

Stabilizing the spin vortex crystal phase in two-dimensional iron-based superconductors

Joseph O'Halloran, D.F. Agterberg, M.X. Chen, and M. Weinert
Department of Physics, University of Wisconsin–Milwaukee, Milwaukee, Wisconsin 53201, USA
(Dated: December 12, 2016)

We present an investigation of the magnetic structure for iron-based superconductors (FeSCs) when inversion symmetry is broken, such as in substrate-supported monolayers or in the presence of a c-axis electric field. We perform group-, mean-field-, and density-functional-theoretic analyses on a model system of monolayer iron selenide (FeSe) on a strontium titanate ($SrTiO_3(001)$) substrate. Our group- and mean-field-theoretic calculations are more generally applicable to thin films of the rest of the 11 (e.g., FeSe) family of iron-based superconductors, as well as to thin films of the 111 (e.g., LiFeAs) and 1111 (e.g., LaOFeAs) families, as these all belong to the same space group. We find that in systems with a collinear antiferromagnetic phase in bulk, when inversion symmetry is broken the transition is instead into a "spin vortex crystal" phase, and that a further phase transition can occur at a lower temperature in some circumstances. The spin vortex crystal is a C_4 symmetric magnetic phase which is related to this parent C_2 symmetric collinear antiferromagnetic (stripe) phase which is ubiquitous among the iron-based superconductors.

I. INTRODUCTION

Following their discovery, there has been much interest in iron-based superconductors (FeSCs), which have a rich phase diagram showing nematic, magnetic, and superconducting orders[1–4]. In particular, monolayer iron selenide (FeSe) shows an as of yet unexplained enhancement in superconducting critical temperature to high temperatures[5–8]. Since magnetic fluctuations compete with superconductivity, a description of the superconducting pairing mechanism relies critically on an understanding of the magnetic fluctuations[9]. While most of the iron-based superconductors exhibit an antiferromagnetic stripe order[2], bulk FeSe appears to be paramagnetic[10]. This has led others to investigate various magnetic configurations to compete with the C_2 stripe order (alternatively, collinear or single-$\boldsymbol{q}$), particularly C_4 (alternatively, tetragonal or double-$\boldsymbol{q}$) orders, which have been given various labels; orthomagnetic (OM) and spin charge order (SCO)[11–14], C_4 spin density wave (SDW)[15], spin vortex crystal (SVC) and charge-spin density wave (CSDW)[16–18]. The orthomagnetic order is equivalent to the spin vortex crystal, while the spin charge order is equivalent to the charge-spin density wave. In this paper, we use the terminology spin vortex crystal and charge-spin density wave. We also will use single- and double-$\boldsymbol{q}$ as broader descriptors. The wavevectors $\boldsymbol{q}$ used in describing the single- and double-$\boldsymbol{q}$ states are expressed differently in the 1- and 2-Fe unit cell descriptions of FeSe, but join the corresponding Brillouin zone center to the point on the Brillouin zone boundary around which electron pockets are typically found.

Inversion symmetry breaking can be accomplished by looking at thin films supported by substrates or in an electric field directed along the c-axis. We consider, then, the effect that inversion symmetry breaking has on the different magnetic structures introduced above. In particular, we find that when an inversion symmetric bulk crystal has a stripe antiferromagnetic ground state, the same material with broken inversion symmetry will instead transition into the spin vortex crystal, with a possible second magnetic transition at lower temperatures. While bulk FeSe does not show long-range magnetic order, the magnetic ground state of monolayer FeSe has not yet been determined, and it is possible that the spin vortex state will be observed in FeSe. However, since many of the iron-based superconductors share the same crystal symmetries with FeSe, it may be possible to observe the spin vortex crystal in many thin-films grown on a substrate or in a c-axis electric field.

By considering the space group symmetry of substrate supported monolayer FeSe, we investigate the effects of inversion symmetry breaking (thin films or under electric field) on the magnetic states in the 11 (FeSe), 111 (LiFeAs), and 1111 (LaOFeAs) families of iron-based superconductors, all of whose bulk crystal structures have P4/nmm symmetry. We show that two-dimensional irreducible representations of the group are split upon breaking inversion symmetry, the result of which is the stabilization of a spin vortex crystal order. This is further supported by mean-field calculations, which confirms a transition from a paramagnetic state into a spin vortex crystal, but which finds there can be an additional transition to a magnetic state intermediary between the stripe antiferromagnet and the spin vortex crystal. We also perform zero-temperature density-functional calculations on free-standing and substrate supported monolayers of iron-selenide, where we find that the spin vortex crystal is more stable on the substrate, but not identified as the ground state.

The spin vortex crystal phase is also intrinsically interesting as it has the same structure as a magnetic skyrmion lattice. Lone skyrmions and skyrmion lattices are often found in materials lacking inversion symmetry and possessing strong spin-orbit coupling[19], and are a topic of interest in spintronics[20–22], as well as in studying the anomalous hall effect[23]. The spin vortex crystal structure is a Néel antiferroskyrmion, where adja-

cent skyrmion sites have opposite chirality, and where the skyrmion radius is on the order of 1.8 Å (i.e., half a lattice spacing of a 2-Fe unit cell).

This work begins by describing each of the magnetic structures in Sec. II; there are three energetically distinct single-$\boldsymbol{q}$ structures – two with moments perpendicular to the c-axis, one with moments parallel to the c-axis; each having two degenerate modes – and for each degenerate pair of single-$\boldsymbol{q}$ states, there is a corresponding pair of double-$\boldsymbol{q}$ states, themselves being superpositions of the single-$\boldsymbol{q}$ states.

Sec. III gives a brief overview of the group structure, following the work of Cvetkovic and Vafek[24], and the representations to which each of the magnetic states belong. We then discuss how breaking inversion symmetry, as our model system does, causes some irreducible representations to become reducible, resulting in formerly degenerate magnetic states becoming non-degenerate with different transition temperatures.

In Sec. IV we investigate a Ginzburg-Landau free energy for the magnetic ground state, and we show that some single-$\boldsymbol{q}$ ground states, those with moments perpendicular to the c-axis, are forced to become double-$\boldsymbol{q}$ states when inversion symmetry is broken, and that the splitting in transition temperatures between states can lead to there being two magnetic transitions. Various reports[12,16,25,26] have done similar mean field calculations, but for bulk crystals with inversion symmetry, while this work considers the case with inversion symmetry no longer present.

Then, Sec. V details density-functional calculations for the different magnetic structures. To verify the stabilization of the spin vortex crystal, we compare calculations on free-standing (inversion symmetric) monolayer FeSe with those for FeSe on a titanium dioxide ($TiO_2(001)$) substrate. We observe the spin vortex crystal to be metastable and find an estimate on the strength of the spin-orbit coupling.

Finally, Sec. VI presents some considerations for further experiments. We discuss some of the limitations of density-functional calculations and the viability of finding the spin vortex phase in FeSe itself; instead, other pnictides/chalcogenides present better candidates for observing this phase.

II. MAGNETIC STRUCTURES

It has been shown that single electron spin-orbit coupling in iron-based superconductors is strong[27](approximately 10.7 meV), and neutron scattering experiments suggest that this single electron spin-orbit coupling reveals itself in the magnetic excitation spectrum; a spin-space anisotropy exists to around 6–8 meV[28,29]. Additionally, our density-functional-theory calculations, discussed in Sec. V, indicate a preferred spin direction which is approximately 1.5 meV/Fe lower in energy than either orthogonal direction. In light of this, we can consider a theory of magnetism in which the SU(2) spin rotation symmetry is not present, and we will later consider order parameters where this is the case.

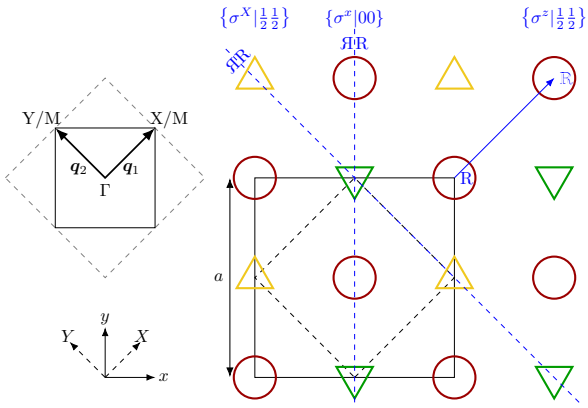

FIG. 1. The two dimensional crystal structure of FeSe, the model system for our investigation. The trilayer structure consists of a central plane of Fe (red, circles) atoms, puckered by Se above (yellow, upward triangles) and below (green, downward triangles). The 1-Fe (dashed line) and 2-Fe (solid line) unit cells, projected in two dimensions, are highlighted with corresponding Brillouin zones (inset, upper left). The lattice constant for the 2-Fe unit cell is a, while for the 1-Fe square unit cell the lattice constant is $\frac{a}{\sqrt{2}}$ (the 2-Fe unit cell is sometimes referred to as the $\sqrt{2}\times\sqrt{2}$ cell for this reason). The wavevectors $\boldsymbol{q}_1$ and $\boldsymbol{q}_2$ are the same vectors regardless of the choice of unit cell. However, while they are written as $\boldsymbol{q}_1=(\pi,0)$, $\boldsymbol{q}_2=(0,\pi)$ in the 1-Fe unit cell, they are written as $\boldsymbol{q}_1=(\pi,\pi)$, $\boldsymbol{q}_2=(\pi,-\pi)$ for the 2-Fe unit cell, which is the choice we make for this paper. The points X and Y in the 1-Fe unit cell are mapped to equivalent M points in the 2-Fe unit cell. Also pictured are the symmetry operations used as group generators for P4/nmm.

The single- and double-$\boldsymbol{q}$ structures are so called because the moments on the iron sites can be described by a plane wave of spin density with one or two non-zero magnetic ordering vectors, respectively. That is, for the double-$\boldsymbol{q}$ structure we can write the magnetic moment $\boldsymbol{M}(\boldsymbol{r})$ on an iron site as

$$\boldsymbol{M}(\boldsymbol{r}) = \boldsymbol{M}_1 e^{i\boldsymbol{q}_1\cdot\boldsymbol{r}} + \boldsymbol{M}_2 e^{i\boldsymbol{q}_2\cdot\boldsymbol{r}}\,, \tag{1}$$

where the ordering vectors $\boldsymbol{q}_1$ and $\boldsymbol{q}_2$ are equivalent but not equal. Some impose certain conditions on the relation between $\boldsymbol{M}_1$ and $\boldsymbol{M}_2$ but do not otherwise fix $\boldsymbol{M}_1$ in any particular direction, but that will not be the case here. Nevertheless, we will use this as a starting point and impose the restrictions due to spin-orbit coupling later.

The single-$\boldsymbol{q}$ state can be described by taking $\boldsymbol{M}_2=0$, which leaves only a single wave vector $\boldsymbol{q}_1$ to describe the wave, which gives rise to a stripe phase. In the spin vortex crystal, $\boldsymbol{M}_1$ is perpendicular to $\boldsymbol{M}_2$, while in the charge-spin density wave phase, $\boldsymbol{M}_1$ and $\boldsymbol{M}_2$ are parallel or anti-parallel. In the case of the iron-based superconductors, the wave vectors are often written $\boldsymbol{q}=(\pi,0)$ or

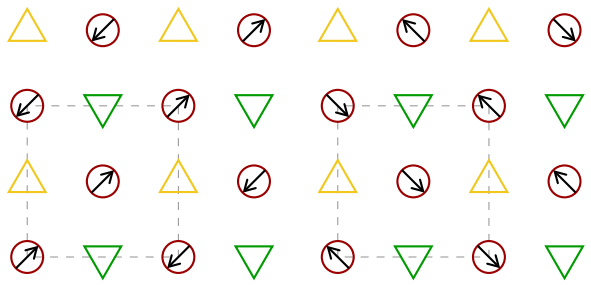

(a) $E^X_{M_2}$ (b) $E^Y_{M_2}$

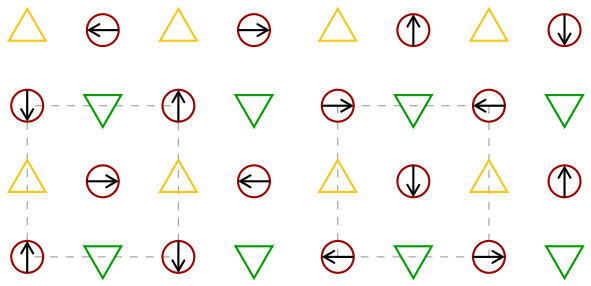

(c) $A_{1,M}$ (d) $B_{2,M}$

FIG. 2. The parallel stripe phases, (a) and (b), and the related spiral spin vortex phases, (c) and (d). The spin vortex structure can be generated by taking the sum and difference of the stripe phases. The moments on the iron sites (red, circles) are indicated by arrows, while the upper (yellow, upward triangle) and lower (green, downward triangle) pnictogen lattices do not carry moments.

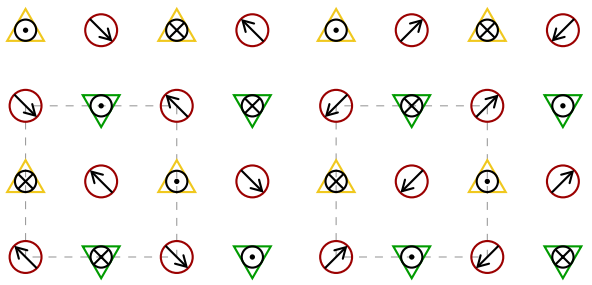

(a) $E^X_{M_1}$ (b) $E^Y_{M_1}$

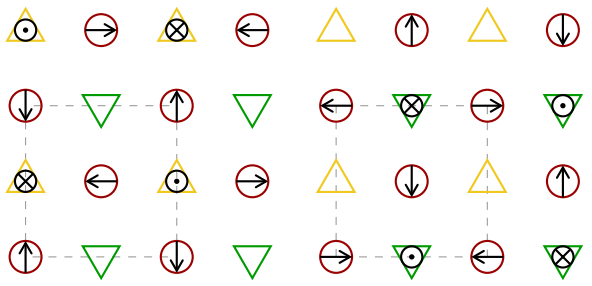

(c) $B_{1,M}$ (d) $A_{2,M}$

FIG. 3. The perpendicular stripe phases, (a) and (b), and the related hedgehog spin vortex phases, (c) and (d). The spin vortex structure can be generated by taking the sum and difference of the stripe phases. For these phases, the moments on the upper (yellow, upward triangle) and lower (green, downward triangle) selenium atoms, are indicated by arrows and directed along the c-axis, perpendicular to the page.

$\boldsymbol{q} = (0, \pi)$ (the X and Y points, respectively), in the Brillouin zone for the 1-Fe unit cell, shown in dashed lines in Fig. 1. For this paper, we use the crystallographic 2-Fe unit cell, shown in solid lines in Fig. 1. In the Brillouin zone for the 2-Fe unit cell, the wave vectors $(\pi, 0)$ and $(0, \pi)$ of the 1-Fe unit cell are instead written as (π, π) and $(-\pi, \pi)$ (equivalent M points), as indicated in Fig. 1. While much work has been done with reference to the 1-Fe unit cell, Nica *et al.*[30] showed the importance of the glide-plane symmetry in allowing the unfolding from a 1-Fe unit cell to a 2-Fe unit cell; this symmetry, and the double degeneracy on the Brillouin zone boundary which allows the unfolding, is absent upon inversion breaking.

We shall now describe the different magnetic structures of interest in this paper. The literature has largely treated the spin vortex crystal state as a single magnetic configuration where the moments on nearest-neighbor iron sites are orthogonal to each other. However, in light of the documented role of spin-orbit coupling, it is helpful to better distinguish all of the magnetic states under consideration. Of the twelve magnetic structures we describe, Fig. 2 shows the first four: the two conjugate "parallel" stripe antiferromagnetic orders ($E^X_{M_2}$; $E^Y_{M_2}$) which have the iron site moments directed parallel to the direction of the stripe, and the two "spiral" spin vortex crystal states ($A_{1,M}$; $B_{2,M}$), which are taken as the sum or difference of the two parallel stripes. We are labeling these states as spiral spin vortex crystal states because the moments on the iron atoms exhibit the same magnetic structure as a spiral magnetic skyrmion. When inversion symmetry is present, the spiral spin vortex crystal states are also degenerate. However, we shall show in Sec. III that breaking inversion symmetry lifts this degeneracy, and further that the spin vortex crystal becomes the stable configuration.

Fig. 3 shows the next set of related states: the two conjugate "perpendicular" stripe antiferromagnetic orders ($E^X_{M_1}$; $E^Y_{M_1}$), which have in plane moments directed perpendicular to the direction of the stripe on the iron sites, and the two "hedgehog" spin vortex crystal states ($B_{1,M}$; $A_{2,M}$), which are taken as the sum or difference of the two perpendicular stripes. Note that in Fig. 3 there are induced moments on the pnictogen/chalcogen sites, whereas in Fig. 2 these induced moments are not present. These moments are required by symmetry, as was shown to be the case by Cvetkovic and Vafek[24]. The induced moments could be potentially seen by a local probe, and would appear as an out of plane canting of magnetic moments near, but away from, an iron site. The similarity

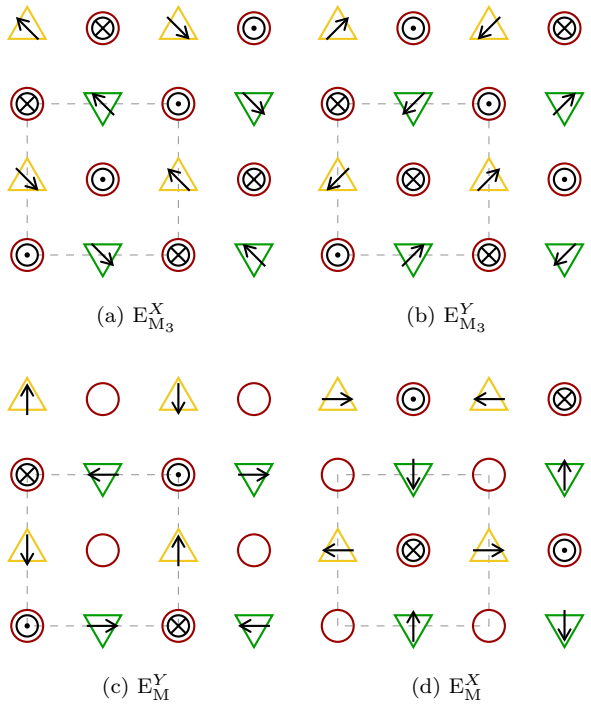

(a) $E^X_{M_3}$ (b) $E^Y_{M_3}$

(c) E^Y_M (d) E^X_M

FIG. 4. The c-axis stripe phases, (a) and (b), and the related charge-spin density wave phases, (c) and (d). The charge-spin density waves can be generated by taking the sum and difference of the stripe phases. The charge-spin density wave should not be confused with a Néel antiferromagnet; the charge-spin density wave is a double-$\boldsymbol{q}$ spin density wave with $\boldsymbol{q}$ at M, whereas the Néel antiferromagnet (checkerboard order) is a single-$\boldsymbol{q}$ spin density wave with $\boldsymbol{q}$ at Γ.

to the hedgehog skyrmion structure is more apparent due to the presence of moments on the pnictogen/chalcogen sites.

We also have stripe phases with moments on the iron sites directed out of the plane, shown in Fig. 4, with their corresponding double-$\boldsymbol{q}$ states. Again, there are two conjugate "c-axis" stripe phases ($E^X_{M_3}$; $E^Y_{M_3}$), and the C_4 symmetric states which accompany them have been called charge-spin density waves[16] (E^Y_M; E^X_M). We shall show in Sec. III that contrary to both of the in-plane stripe phases, the c-axis stripe phases remain degenerate even after inversion symmetry is broken.

We also note that in principle, there can be some arbitrary linear combination of conjugate single- or double-$\boldsymbol{q}$ states which produces a generally mixed state with moments deviating from the single-$\boldsymbol{q}$ state by some angle θ, an example of which is shown in Fig. 5 which mixes the perpendicular stripe phases. The resulting states are C_2 symmetric, and we refer to them collectively as the "mixed" state.

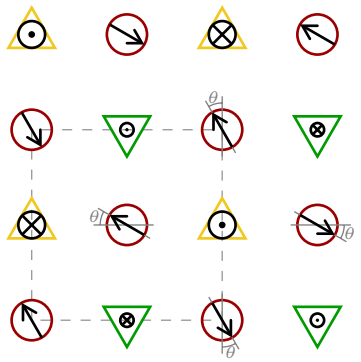

FIG. 5. An example of the in-plane canted moments in a mixed state. This can result if stripe (or vortex) phases are unevenly mixed — here we have an uneven mixing of the $B_{1,M}$ and $A_{2,M}$ hedgehog spin vortex crystal; equivalently, and uneven mixing of the $E^X_{M_1}$ and $E^Y_{M_1}$ perpendicular stripe antiferromagnetic phase.

III. GROUP STRUCTURE

The space group to which the 11, 111, and 1111 families of iron-based superconductors belong is P4/nmm. As shown in Fig. 1, P4/nmm has three group generators; $\{\sigma^X|\frac{1}{2}\frac{1}{2}\}$, a mirror plane through the origin (center of the unit cell) perpendicular to the X axis followed by a translation by $(\frac{a}{2},\frac{a}{2},0)$; $\{\sigma^x|00\}$, a mirror plane through the origin, perpendicular to the x axis with no additional translation; and $\{\sigma^z|\frac{1}{2}\frac{1}{2}\}$, a mirror plane through the origin, perpendicular to the z axis, followed by a translation by $(\frac{a}{2},\frac{a}{2},0)$. It is this last element, $\{\sigma^z|\frac{1}{2}\frac{1}{2}\}$, which generates the inversion symmetry, and it is this last element which is removed when we consider a monolayer on a substrate. Note that the specific translations depend upon the choice of origin; indeed, P4/nmm is non-symmorphic, meaning no choice of origin can eliminate translations from every group element (that is, all of the generators). However, when inversion symmetry is broken, the resulting group is P4mm, which is symmorphic.

The stripe and spin vortex crystal orders are described by representations of P4/nmm at the M-point, summarized in table I. The parallel stripes belong to the overall symmetry E_{M_2}; if we take the structure depicted in Fig. 2a, and perform the group operation $\{\sigma^X|\frac{1}{2}\frac{1}{2}\}$, the structure is unchanged. However, the result of $\{\sigma^x|00\}$ is the structure in figure 2b. Similarly, one can verify that the perpendicular stripes in Fig. 3a–3b belong to E_{M_1}, while the c-axis stripes in Fig. 4a–4b belong to E_{M_3}. While an E_{M_4} order could be supported, there would not be any moments on the iron sites. A word of reminder: spins transform as axial vectors — pseudovectors — acquiring an additional sign change under improper rotations, unlike the arrows used to represent the spins.

When we break inversion, that is, when we remove the

$\mathbf{P}_{\mathrm{M}}$	$\{\sigma_X\vert\frac{1}{2}\frac{1}{2}\}$	$\{\sigma_x\vert 00\}$	$\{\sigma_z\vert\frac{1}{2}\frac{1}{2}\}$
$\mathrm{E}_{\mathrm{M}_1}$	$\begin{bmatrix}-1 & 0\\ 0 & -1\end{bmatrix}$	$\begin{bmatrix}0 & 1\\ 1 & 0\end{bmatrix}$	$\begin{bmatrix}-1 & 0\\ 0 & 1\end{bmatrix}$
$\mathrm{E}_{\mathrm{M}_2}$	$\begin{bmatrix}1 & 0\\ 0 & 1\end{bmatrix}$	$\begin{bmatrix}0 & 1\\ 1 & 0\end{bmatrix}$	$\begin{bmatrix}-1 & 0\\ 0 & 1\end{bmatrix}$
$\mathrm{E}_{\mathrm{M}_3}$	$\begin{bmatrix}1 & 0\\ 0 & -1\end{bmatrix}$	$\begin{bmatrix}0 & 1\\ 1 & 0\end{bmatrix}$	$\begin{bmatrix}-1 & 0\\ 0 & 1\end{bmatrix}$
$\mathrm{E}_{\mathrm{M}_4}$	$\begin{bmatrix}-1 & 0\\ 0 & 1\end{bmatrix}$	$\begin{bmatrix}0 & 1\\ 1 & 0\end{bmatrix}$	$\begin{bmatrix}-1 & 0\\ 0 & 1\end{bmatrix}$

TABLE I. Irreducible representations at the M point for the group generators. The basis used treats the single-$\boldsymbol{q}$ phases depicted in Sec. II as basis functions; the double-$\boldsymbol{q}$ phases act as basis functions for a rotated basis in their respective representations.

generator $\{\sigma^z\vert\frac{1}{2}\frac{1}{2}\}$, we notice that the transformation

$$U_1 = \frac{1}{\sqrt{2}}\begin{pmatrix}1 & 1\\ -1 & 1\end{pmatrix} \tag{2}$$

diagonalizes the remaining representations for $\mathrm{E}_{\mathrm{M}_1}$ and $\mathrm{E}_{\mathrm{M}_2}$, meaning absent inversion symmetry the representations are reducible - and the states they describe are no longer degenerate. However, $\mathrm{E}_{\mathrm{M}_3}$ and $\mathrm{E}_{\mathrm{M}_4}$ remain irreducible, although they do become equivalent under

$$U_2 = \begin{pmatrix}0 & 1\\ 1 & 0\end{pmatrix}. \tag{3}$$

This is a result of transitioning from a non-symmorphic group to a symmorphic one, which forces the representations at the M-point become those of the point group $\mathrm{C}_{4\mathrm{V}}$, as shown in table II, which is the same point group representation as for the Γ-point. The formerly irreducible representations $\mathrm{E}_{\mathrm{M}_1}$ and $\mathrm{E}_{\mathrm{M}_2}$ now reduce to the representations $\mathrm{A}_{2,\mathrm{M}} \oplus \mathrm{B}_{1,\mathrm{M}}$ and $\mathrm{A}_{1,\mathrm{M}} \oplus \mathrm{B}_{2,\mathrm{M}}$ respectively. Because of the change of basis represented by U_1, the spiral spin vortex phase in Fig. 2c belongs to the $\mathrm{A}_{1,\mathrm{M}}$ representation, while the conjugate phase, 2d, belongs to the $\mathrm{B}_{2,\mathrm{M}}$ representation, and the hedgehog spin vortex phase in Fig. 3c belongs to the $\mathrm{B}_{1,\mathrm{M}}$ representation, while the conjugate phase, 3d, belongs to the $\mathrm{A}_{2,\mathrm{M}}$ representation.

$\widetilde{\mathbf{P}}_{\mathrm{M}}$	$\{\sigma_X\vert\frac{1}{2}\frac{1}{2}\}$	$\{\sigma_x\vert 00\}$
$\mathrm{A}_{1,\mathrm{M}}$	1	1
$\mathrm{A}_{2,\mathrm{M}}$	−1	−1
$\mathrm{B}_{1,\mathrm{M}}$	−1	1
$\mathrm{B}_{2,\mathrm{M}}$	1	−1
E_{M}	$\begin{bmatrix}-1 & 0\\ 0 & 1\end{bmatrix}$	$\begin{bmatrix}0 & 1\\ 1 & 0\end{bmatrix}$

TABLE II. Irreducible representations at the M point lacking inversion symmetry for the group generators.

It is perhaps interesting to note that a number of experiments have found evidence of the C_4 symmetric charge-spin density wave in hole doped Ba122 compounds[31–36]. The space group of $BaFe_2As_2$, and indeed the 122 family, is I4/mmm, which is symmorphic, and we have seen that P4/nmm becomes symmorphic upon inversion symmetry breaking, stabilizing the C_4 symmetric spin vortex crystal.

IV. MEAN-FIELD THEORY

Now that we have a identified the magnetic structures under discussion, and the group representations to which they belong, we shall provide a Ginzburg-Landau analysis which respects the symmetries present. Before we begin, however, we should note recent works[16,18,26], which use a free energy functional

$$F[\boldsymbol{M}_i] = a(\boldsymbol{M}_1^2+\boldsymbol{M}_2^2) + \frac{u}{2}(\boldsymbol{M}_1^2+\boldsymbol{M}_2^2)^2 - \frac{g}{2}(\boldsymbol{M}_1^2-\boldsymbol{M}_2^2)^2 + 2w(\boldsymbol{M}_1\cdot\boldsymbol{M}_2)^2 \tag{4}$$

This expression is for the free energy of a spin density wave $\boldsymbol{S}(\boldsymbol{r}) = \boldsymbol{M}_1 e^{i\boldsymbol{Q}_1\cdot\boldsymbol{r}} + \boldsymbol{M}_2 e^{i\boldsymbol{Q}_2\cdot\boldsymbol{r}}$ where $\boldsymbol{M}_1$ and $\boldsymbol{M}_2$ belong to an E_{M} representation, but remain globally rotationally invariant. In this work, we are chiefly concerned with the evolution from either of the two in-plane stripe phases to the spin vortex crystal with spin-orbit coupling, which gives order parameters η_X and η_Y that transform as $\mathrm{E}^X_{\mathrm{M}_i}$ and $\mathrm{E}^Y_{\mathrm{M}_i}$, respectively, but which are no longer invariant to continuous rotations. That is, rather than investigate competition between the single- and double-$\boldsymbol{q}$ phases, we assume that the ground state prior to inversion breaking is one of the stripe phases. Therefore, our analysis does not strictly apply to iron-based superconductors which do not show stripe ordering in their bulk magnetic structure. In particular, this means the theory is of limited applicability to FeSe itself. However, early calculations of magnetism in LaOFeAs — which does show bulk stripe antiferromagnetism — found an unspecified spin vortex crystal upon increasing the Fe-As layer distance[37], suggesting this is a good candidate to observe the spin vortex crystal experimentally.

The free energy for the representations at the M-point, when inversion symmetry is present, is given by

$$f = \alpha(\eta_X^2+\eta_Y^2) + \beta_1(\eta_X^2+\eta_Y^2)^2 + \beta_2\eta_X^2\eta_Y^2, \tag{5}$$

where η_X and η_Y transform as $\mathrm{E}^X_{\mathrm{M}_i}$ and $\mathrm{E}^Y_{\mathrm{M}_i}$, respectively, and $\alpha = \alpha^0(t-t_c)$, with $\alpha^0 > 0$ and t, t_c are dimensionless temperatures. This has the same form as the free energy in equation (4) for the case that $\boldsymbol{M}_1\cdot\boldsymbol{M}_2 = 0$, with $u = 2\beta_1 + \frac{\beta_2}{2}$ and $g = \frac{\beta_2}{2}$. To see the effects of inversion breaking, consider Table I. In particular, we note that under $\{\sigma_z\vert\frac{1}{2}\frac{1}{2}\}$,

$$\eta_X \to -\eta_X$$
$$\eta_Y \to +\eta_Y .$$

When inversion symmetry is broken, $\{\sigma_z|\frac{1}{2}\frac{1}{2}\}$ is no longer present, and the free energy describing states with $\mathrm{E_{M_1}}$ or $\mathrm{E_{M_2}}$ symmetry has additional terms carrying the product $\eta_X\eta_Y$, which are clearly not allowed with inversion symmetry present – or for states with $\mathrm{E_{M_3}}$ or $\mathrm{E_{M_4}}$ symmetry, as such terms are precluded by $\{\sigma_X|\frac{1}{2}\frac{1}{2}\}$. The resulting free energy is:

$$\begin{aligned}\widetilde{f} =&\alpha(\eta_X^2+\eta_Y^2)+\beta_1(\eta_X^2+\eta_Y^2)^2+\beta_2\eta_X^2\eta_Y^2\\ &+\widetilde{\alpha}\eta_X\eta_Y+\beta_3\eta_X\eta_Y(\eta_X^2+\eta_Y^2)\,. \end{aligned}\tag{6}$$

Compared to equation (5), we have $\widetilde{f}=f+\widetilde{\alpha}\eta_X\eta_Y+\beta_3\eta_X\eta_Y(\eta_X^2+\eta_Y^2)$. Since the transformation matrix U_1 given in equation (2) diagonalizes both $\mathrm{E_{M_1}}$ and $\mathrm{E_{M_2}}$, we make the substitution $\eta_\pm=\frac{1}{\sqrt{2}}(\eta_X\pm\eta_Y)$ to recast equation (6) as

$$\widetilde{f}=\alpha_+\eta_+^2+\alpha_-\eta_-^2+\beta_+\eta_+^4+\beta_-\eta_-^4+\beta_m\eta_+^2\eta_-^2\,. \tag{7}$$

We can take $\alpha_+=\alpha^0(t-1)$ and $\alpha_-=\alpha^0(t-1+\delta)$ and we have scaled temperature so that $t_c^+=1$. Requiring that the free energy be bounded below introduces the restrictions $\beta_\pm>0$ and either $\beta_m>0$ or $-2\sqrt{\beta_+\beta_-}<\beta_m<0$. It can be shown that $\delta=(T_c^+-T_c^-)/T_c^+=-\widetilde{\alpha}/\alpha^0$; without loss of generality, we assume $\widetilde{\alpha}<0$, that is, $\delta>0$. This is not a minor point; the transition temperature for the magnetic state is split by breaking inversion symmetry because spin vortex crystal states which were formally part of the same 2D irreducible representation (e.g., $\mathrm{E_{M_1}}$) now belong to different 1D irreducible representations (e.g., $\mathrm{A_{2,M}}$ and $\mathrm{B_{1,M}}$), which means absent fine tuning they will have different transition temperatures. It is on this basis which we can make the claim the spin vortex crystal is stabilized, as some spin vortex crystal phase must order prior to the other.

It is useful to introduce the parameters

$$\begin{aligned}x&=\frac{\beta_m}{2\beta_+}\\ \xi&=\sqrt{\frac{\beta_-}{\beta_+}}\,.\end{aligned}$$

In terms of these, $x<-\xi<0$ is prohibited, as it is equivalent to $\beta_m<-2\sqrt{\beta_+\beta_-}$. We find that the system experiences a second order transition from the paramagnetic state into a spin vortex crystal state ($\mathrm{A_{1,M}}$ or $\mathrm{B_{1,M}}$ under the assumption $\delta>0$) below $t=1$, and a further second order transition into the mixed state at

$$t_c^m=1-\left(\frac{1}{1-x}\right)\delta\,. \tag{8}$$

In the mixed state, because the order parameters grow at different rates, the magnetic phase progresses from the initial spin vortex crystal toward the conjugate spin vortex crystal. We can find that the magnitude of each order parameter is equal along the line

$$t_s=1-\left(\frac{1+x}{1-\xi^2}\right)\delta\,,$$

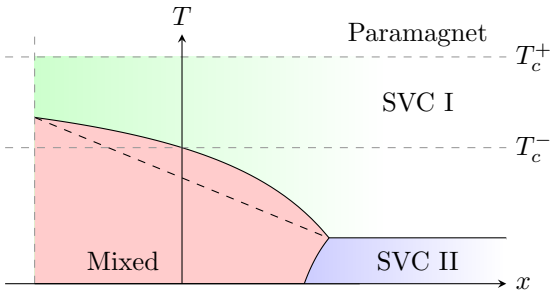

FIG. 6. T-x phase diagram representative of $\xi<1-\delta$. By assumption, without loss of generality, the system initially orders in a spin vortex crystal state ($\mathrm{A_{1,M}}$ spiral or $\mathrm{B_{1,M}}$ hedgehog). The system experiences a second order transition into the ordered but low symmetry "mixed" phase below the line $t_c^m=1-\left(\frac{1}{1-x}\right)\delta$. The dashed line in the mixed region is the line along which both order parameters have the same magnitude, i.e., it is the stripe phase, which is of measure zero. At $x=\xi$ there is a triple point, and the system experiences a first order transition to the conjugate spin vortex crystal ($\mathrm{B_{2,M}}$ spiral or $\mathrm{A_{2,M}}$ hedgehog) below the triple point temperature. If $\xi\geq 1-\delta$, the triple point temperature is less than or equal to zero and the transition to the conjugate spin vortex crystal is completely suppressed.

which is shown as the dashed line in the mixed state in Fig. 6. Since this intersects with the transition t_c^m at $x=\pm\xi$, for $\xi\geq 1-\delta$ the conjugate vortex is suppressed and the stripe phase is absent from a region of the mixed state. For $\xi<1-\delta$, there can also be a transition into the conjugate vortex state. Depending on the value of x, this is second order from the mixed state, or first order from the initial spin vortex crystal; e.g., if the first transition is into the $\mathrm{A_{1,M}}$ spiral spin vortex crystal, the second transition is into the $\mathrm{B_{2,M}}$ spiral spin vortex crystal. Fig. 6 shows a representative diagram for $\xi=0.5$, $\delta=0.4$ ($\xi<1-\delta$) in the x-T plane, while Fig. 7 shows a $T=0$ diagram in the x-ξ plane with $\delta=0.4$.

The parameter ξ can in some sense be thought of as the strength of the mixed state; treating ξ as a free parameter, in the limit $\xi\to 0$ we see that the mixed state vanishes and that the conjugate vortex state orders at T_c^- ($t=1-\delta$ in reduced temperature). Notably, we see that the stripe phase is almost never going to be the ground state.

As noted previously, when the ground state magnetic structure of the inversion symmetric parent compound belongs to the $\mathrm{E_{M_3}}$ representation, breaking inversion symmetry does not lift the degeneracy of this magnetic state. However, it does allow for additional mixing terms which modify the transition temperature because the representations $\mathrm{E_{M_3}}$ and $\mathrm{E_{M_4}}$ become equivalent under the transformation noted in equation 3. If we assume without loss of generality that $\mathrm{E_{M_3}}$ orders, then when inversion symmetry is present, we can write the free energy as

$$f_3=\alpha(\eta_{X_3}^2+\eta_{Y_3}^2)+\beta_1(\eta_{X_3}^2+\eta_{Y_3}^2)^2+\beta_2\eta_{X_3}^2\eta_{Y_3}^2\,, \tag{9}$$

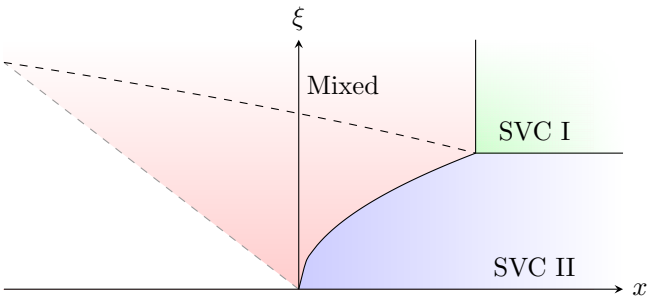

FIG. 7. Zero temperature phase diagram in the x-ξ plane, for $\delta = 0.4$. At large values of ξ the conjugate vortex state is suppressed and the primary vortex state orders to zero temperature. The dashed line in the mixed region represents the stripe phase; below the line $x = -\xi$ the fourth order mean-field theory is no longer applicable.

where η_{X_3} and η_{Y_3} transform as the upper and lower components of $\mathrm{E_{M_3}}$, respectively. We note then, that a term of the form $\eta_{X_3}\eta_{Y_4} + \eta_{X_4}\eta_{Y_3}$ is forbidden by $\{\sigma^z|\frac{1}{2}\frac{1}{2}\}$, but not by the other generators. So, upon breaking inversion symmetry, we get the modified free energy:

$$\widetilde{f}_3 = f_3 + \alpha_m(\eta_{X_3}\eta_{Y_4} + \eta_{X_4}\eta_{Y_3}) + \widetilde{\alpha}(\eta_{X_4}^2 + \eta_{Y_4}^2)\,.$$

Minimizing this free energy with respect to η_{X_4} and η_{Y_4} modifies the term α; the result is

$$f_3 = \left(\alpha - \frac{\alpha_m^2}{4\widetilde{\alpha}}\right)(\eta_{X_3}^2 + \eta_{Y_3}^2) + \beta_1(\eta_{X_3}^2 + \eta_{Y_3}^2)^2 + \beta_2\eta_{X_3}^2\eta_{Y_3}^2\,.$$

The critical temperature for the transition is given by setting the quadratic coefficient to zero.

V. DENSITY-FUNCTIONAL THEORY

Density-functional theory calculations were performed using the Vienna Ab initio Simulation Package.[38,39] The exchange correlation functional is approximated by the generalized gradient approximation as parametrized by Perdew, Burke and Ernzerhof,[40] and the pseudopotentials were constructed by the projector augmented wave method.[41,42] A 33×33 Monkhorst-Pack k-mesh was used to sample the surface BZ and a plane-wave energy cut off of 400 eV was used for structural relaxation and electronic structure calculations.

We performed non-collinear magnetic calculations with spin-orbit coupling included for ideal freestanding monolayer FeSe based on the well relaxed structure. We considered a number of magnetic orders: three single-$\boldsymbol{q}$ states, parallel (Fig. 2a), perpendicular (Fig. 3a), and c-axis stripes (Fig. 4a); and three double-$\boldsymbol{q}$ states, the two hedgehog spin vortex states (Fig. 3c, 3d) and a spiral spin vortex state (Fig. 2c). Our calculations find that the three single-$\boldsymbol{q}$ states are energetically different, with the perpendicular stripe phase having the lowest energy; about 1.6 meV/Fe and 1.5 meV/Fe lower than the parallel and c-axis stripes, respectively. Additionally, the hedgehog spin vortex states are energetically favored over the spiral spin vortex state, again by about 1.6 meV/Fe, which is not surprising as the hedgehog spin vortex belongs to the same representation as the perpendicular stripes when inversion symmetry is present. The spin vortex crystal phases are locally stable and approximately 63 meV/Fe higher than the stripe phases on the freestanding FeSe.

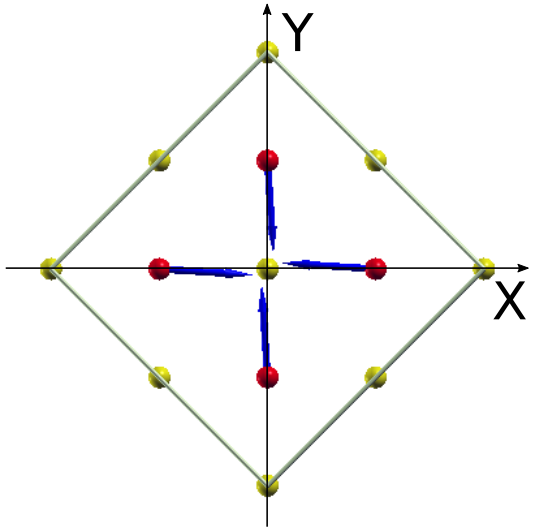

FIG. 8. Magnetization in an FeSe monolayer supported by TiO_2(001). The moments, slightly amplified for clarity, are canted by about 1.5° compared to those for the freestanding FeSe layer. The DFT calculations did not investigate the possibility of moments on Selenium (yellow) atoms. The mixed state observed here matches that as shown in Fig. 5.

To model inversion symmetry breaking, we place the monolayer FeSe on a titanium dioxide single layer. Titanium dioxide is chosen here because it has a small lattice mismatch with FeSe, so that the unit cell for the system has the same in plane lattice constants as freestanding FeSe. Our calculations find that the substrate has a tendency to stabilize the spin vortex phase, that is, the energy differences between the stripe phases and the spin vortex phases are significantly decreased to about 45 meV/Fe. We also observe a small energy difference between the hedgehog spin vortex crystal and its conjugate hedgehog state, as expected since the two states belong to separate representations when inversion symmetry is broken. Additionally, the substrate has noticeable effects on the spin vortex structure; for the freestanding monolayer, DFT calculations for the spin vortex structure find a local minimum for the hedgehog spin vortex, however, for the supported monolayer the local minimum exhibits a canting of about 1.5° away from the hedgehog spin vortex phase, shown in Fig. 8, in accordance with the mixed phase exhibited in Fig. 5.

The mean-field analysis indicates that the canting angle observed in our DFT measurements should be a func-

tion of temperature, but DFT is done at zero temperature and we do not observe temperature evolution of the mixed state for that reason. Furthermore, DFT also does not find the finite temperature window over which the pure spin vortex crystal exists. We also note that at zero temperature, there is a broad region which allows the mixed phase, as indicated in Fig. 7, however, much depends on the material dependent parameters identified earlier, and we cannot tell from the DFT calculations which spin vortex state would order first, nor where on the zero temperature x-ξ diagram we would expect the system to be.

VI. CONSIDERATIONS FOR EXPERIMENT

Our DFT calculations still predict a ground state of stripe antiferromagnetism, but a number of caveats should be borne in mind. To begin, DFT calculations can sometimes predict the wrong magnetic ground state, as in the case of chromium[43], however, the empirical ground state is identified by DFT as at least being metastable. Indeed, in the case of bulk FeSe, the lowest energy magnetic order is stripe antiferromagnetism, contrary to experimental evidence of paramagnetism persisting to low temperatures. Next, DFT calculations which use a Néel antiferromagnetic structure produce band structures which have the best agreement with experimentally observed band structures, although it is not energetically favored[44]. Additionally, DFT calculations of magnetic states in iron-based superconductors are highly sensitive to structural and calculational details[45]. Under those considerations, we suggest that the exact numbers reported here are less important than the facts that the relative energy difference between the stripe and spin vortex phases decreases significantly when inversion symmetry is broken, and that the spin vortex phases are locally stable.

While our analysis used monolayer FeSe on a $SrTiO_3$ substrate as our model system, we acknowledge that it is not a strong candidate to observe the effect, due to the paramagnetic behavior of the bulk material. The spin vortex crystal is still a possibility in monolayer FeSe, but we expect that materials which clearly show stripe antiferromagnetism in the bulk to be the best candidates to observe the spin vortex crystal upon breaking inversion symmetry. Ultra-thin films of LaOFeAs or NaFeAs, for example, subject to a c-axis electric field should transition into the spin vortex crystal phase from the paramagnetic phase, and may have a further transition at lower temperatures still.

VII. CONCLUSIONS

Thus, we have determined that, for iron-based superconductors which in the bulk both belong to P4/nmm, namely the 11, 111, and 1111 families of iron-based superconductors, and exhibit a collinear in-plane stripe phase, the spin vortex crystal is unavoidable for a finite temperature window when inversion symmetry is broken. As such, the spin vortex crystal should be found in 2D materials or under application of electric fields. Furthermore, in many compounds we expect there to be two magnetic transitions as we approach low temperatures. The parametrization x which we have used will be material dependent, and may depend on such things as doping or pressure. However, for a given material we expect that upon lowering temperature a transition to the spin vortex crystal will occur, which will either persist to zero temperature or experience a second transition.

This work supported by the National Science Foundation grant DMR-1335215.

[1] G. R. Stewart, Rev. Mod. Phys. **83**, 1589 (2011).
[2] A. Chubukov and P. J. Hirschfeld, Phys. Today **68**, 46 (2015).
[3] J.-F. Ge, Z.-L. Liu, C. Liu, C.-L. Gao, D. Qian, Q.-K. Xue, Y. Liu, and J.-F. Jia, Nat. Mater. **14**, 285 (2014).
[4] Q. Si, R. Yu, and E. Abrahams, Nat. Rev. Mater. **1**, 16017 (2016).
[5] S. He, J. He, W. Zhang, L. Zhao, D. Liu, X. Liu, D. Mou, Y.-B. Ou, Q.-Y. Wang, Z. Li, L. Wang, Y. Peng, Y. Liu, C. Chen, L. Yu, G. Liu, X. Dong, J. Zhang, C. Chen, Z. Xu, X. Chen, X. Ma, Q. Xue, and X. J. Zhou, Nat. Mater. **12**, 605 (2013).
[6] D.-H. Lee, Chin. Phys. B **24**, 117405 (2015).
[7] Y. Miyata, K. Nakayama, K. Sugawara, T. Sato, and T. Takahashi, Nat. Mater. **14**, 775 (2015).
[8] S. Coh, M. L. Cohen, and S. G. Louie, New J. Phys. **17**, 073027 (2015).
[9] P. Dai, J. Hu, and E. Dagotto, Nat. Phys. **8**, 709 (2012).
[10] Q. Wang, Y. Shen, B. Pan, X. Zhang, K. Ikeuchi, K. Iida, A. D. Christianson, H. C. Walker, D. T. Adroja, M. Abdel-Hafiez, X. Chen, D. A. Chareev, A. N. Vasiliev, and J. Zhao, Nat. Commun. **7**, 12182 (2016).
[11] J. Lorenzana, G. Seibold, C. Ortix, and M. Grilli, Phys. Rev. Lett. **101**, 186402 (2008).
[12] P. M. R. Brydon, J. Schmiedt, and C. Timm, Phys. Rev. B **84**, 214510 (2011).
[13] M. N. Gastiasoro and B. M. Andersen, Phys. Rev. B **92**, 140506(R) (2015).
[14] G. Giovannetti, C. Ortix, M. Marsman, M. Capone, J. van den Brink, and J. Lorenzana, Nat. Commun. **2**, 398 (2011).
[15] J. Kang, X. Wang, A. V. Chubukov, and R. M. Fernandes, Phys. Rev. B **91**, 121104(R) (2015).
[16] M. Hoyer, R. M. Fernandes, A. Levchenko, and J. Schmalian, Phys. Rev. B **93**, 144414 (2016).
[17] R. M. Fernandes, S. A. Kivelson, and E. Berg, Phys. Rev. B **93**, 014511 (2016).
[18] M. H. Christensen, J. Kang, B. M. Andersen, I. Eremin,

and R. M. Fernandes, Phys. Rev. B **92**, 214509 (2015).
[19] S. Mühlbauer, B. Binz, F. Jonietz, C. Pfleiderer, A. Rosch, A. Neubauer, R. Georgii, and P. Böni, Science **323**, 915 (2009).
[20] A. Tonomura, X. Yu, K. Yanagisawa, T. Matsuda, Y. Onose, N. Kanazawa, H. S. Park, and Y. Tokura, Nano Lett. **12**, 1673 (2012).
[21] A. Fert, V. Cros, and J. Sampaio, Nat. Nanotechnol. **8**, 152 (2013).
[22] N. Romming, C. Hanneken, M. Menzel, J. E. Bickel, B. Wolter, K. v. Bergmann, A. Kubetzka, and R. Wiesendanger, Science **341**, 636 (2013).
[23] N. Nagaosa, J. Sinova, S. Onoda, A. H. MacDonald, and N. P. Ong, Rev. Mod. Phys. **82**, 1539 (2010).
[24] V. Cvetkovic and O. Vafek, Phys. Rev. B **88**, 134510 (2013).
[25] I. Eremin and A. V. Chubukov, Phys. Rev. B **81**, 024511 (2010).
[26] M. H. Christensen, J. Kang, B. M. Andersen, and R. M. Fernandes, Phys. Rev. B **93**, 085136 (2016).
[27] S. V. Borisenko, D. V. Evtushinsky, Z.-H. Liu, I. Morozov, R. Kappenberger, S. Wurmehl, B. Büchner, A. N. Yaresko, T. K. Kim, M. Hoesch, and others, Nat. Phys. **12**, 311 (2016).
[28] P. Steffens, C. H. Lee, N. Qureshi, K. Kihou, A. Iyo, H. Eisaki, and M. Braden, Phys. Rev. Lett. **110** (2013), 10.1103/PhysRevLett.110.137001.
[29] M. Ma, P. Bourges, Y. Sidis, Y. Xu, S. Li, B. Hu, J. Li, F. Wang, and Y. Li, arXiv:1610.01277 [cond-mat] (2016), arXiv: 1610.01277.
[30] E. M. Nica, R. Yu, and Q. Si, Phys. Rev. B **92**, 174520 (2015).
[31] M. G. Kim, A. Kreyssig, A. Thaler, D. K. Pratt, W. Tian, J. L. Zarestky, M. A. Green, S. L. Bud'ko, P. C. Canfield, R. J. McQueeney, and A. I. Goldman, Phys. Rev. B **82**, 220503(R) (2010).
[32] E. Hassinger, G. Gredat, F. Valade, S. R. de Cotret, A. Juneau-Fecteau, J.-P. Reid, H. Kim, M. A. Tanatar, R. Prozorov, B. Shen, H.-H. Wen, N. Doiron-Leyraud, and L. Taillefer, Phys. Rev. B **86**, 140502(R) (2012).
[33] S. Avci, O. Chmaissem, S. Rosenkranz, J. M. Allred, I. Eremin, A. V. Chubukov, D.-Y. Chung, M. G. Kanatzidis, J.-P. Castellan, J. A. Schlueter, H. Claus, D. D. Khalyavin, P. Manuel, A. Daoud-Aladine, and R. Osborn, Nat. Commun. **5** (2014), 10.1038/ncomms4845.
[34] J. M. Allred, K. M. Taddei, D. E. Bugaris, M. J. Krogstad, S. H. Lapidus, D. Y. Chung, H. Claus, M. G. Kanatzidis, D. E. Brown, J. Kang, R. M. Fernandes, I. Eremin, S. Rosenkranz, O. Chmaissem, and R. Osborn, Nat. Phys. **12**, 493 (2016).
[35] J. M. Allred, S. Avci, D. Y. Chung, H. Claus, D. D. Khalyavin, P. Manuel, K. M. Taddei, M. G. Kanatzidis, S. Rosenkranz, R. Osborn, and O. Chmaissem, Phys. Rev. B **92**, 094515 (2015).
[36] A. E. Böhmer, F. Hardy, L. Wang, T. Wolf, P. Schweiss, and C. Meingast, Nat. Commun. **6**, 7911 (2015).
[37] F. Yndurain and J. M. Soler, Phys. Rev. B **79**, 134506 (2009).
[38] G. Kresse and J. Furthmüller, Comput. Mater. Sci. **6**, 15 (1996).
[39] G. Kresse and J. Furthmüller, Phys. Rev. B **54**, 11169 (1996).
[40] J. P. Perdew, K. Burke, and M. Ernzerhof, Phys. Rev. Lett. **77**, 3865 (1996).
[41] P. E. Blöchl, Phys. Rev. B **50**, 17953 (1994).
[42] G. Kresse and D. Joubert, Phys. Rev. B **59**, 1758 (1999).
[43] E. Fawcett, Rev. Mod. Phys. **60**, 209 (1988).
[44] M. X. Chen, D. F. Agterberg, and M. Weinert, arXiv:1603.03841 [cond-mat] (2016), arXiv: 1603.03841.
[45] S. Sharma, J. K. Dewhurst, S. Shallcross, C. Bersier, F. Cricchio, A. Sanna, S. Massidda, E. K. U. Gross, and L. Nordström, arXiv:0810.4278 [cond-mat] (2008), arXiv: 0810.4278.